

# Toward a room temperature Schafroth superconductor based on charged excitonic complexes

Z. Sun<sup>1</sup>, J. Beaumariage<sup>1</sup>, Q. Cao<sup>2</sup>, K. Watanabe<sup>3</sup>,

T. Taniguchi<sup>3</sup>, B. Hunt<sup>2</sup>, I. V. Bondarev<sup>4</sup>, and D. W. Snoke<sup>1</sup>

<sup>1</sup>*Department of Physics and Astronomy, University of Pittsburgh,*

*3941 O'Hara St., Pittsburgh, PA 15260, USA*

<sup>2</sup>*Department of Physics, Carnegie Mellon University 15213, USA*

<sup>3</sup>*National Institute for Materials Science, Tsukuba, Ibaraki 305-0044, Japan*

<sup>4</sup>*Department of Mathematics and Physics, North Carolina Central University,*

*1801 Fayetteville St., Durham, NC 27707, USA*

In 1954, Schafroth proposed a mechanism for superconductivity that is physically possible, but ended up not being the explanation of the well known BCS superconductors. The proposal argued correctly that a Bose condensate of charged bosons should also be a superconductor. In 1996, V.I. Yudson proposed a way to produce a charged boson by attaching two free charges to an exciton in a semiconductor, to make a “quaternion”. While that state was never seen in III-V semiconductors, our calculations show that it is predicted to be stable in structures made with monolayers of transition metal dichalcogenide (TMD) materials. We present experimental spectroscopic measurements that agree with this theory, which indicate that we have observed this charged-boson state in this type of structure. This opens up a new path for pursuing room temperature superconductivity.

In 1996, V.I. Yudson published an intriguing paper [1] in which he proposed the existence of stable four-carrier complexes in bilayer semiconductor structures, which may be called “quaternions.” The geometry considered by Yudson is shown in Figure 1(a). Two semiconductor layers are placed side by side to make a bilayer structure, and this bilayer structure is placed parallel to a nearby metal layer. Under optical pumping, an exciton can be created which then picks up two free electrons (or two holes). At first glance, one would not expect that a complex with three times more negative charge than positive would be stable, although “trions” (two electrons and one hole, or vice versa) are known to be stable in many semiconducting systems [2, 3]. The presence of the metal layer, however, produces image charge below the surface, so that much of the repulsive interaction in the quaternion is canceled out.

Such four-particle complexes are charged bosons: an even number of fermions with a net charge—and therefore will respond to electric field. A Bose-Einstein condensate of these complexes would be a Schafroth superconductor [4]. Schafroth superconductivity was originally proposed as the explanation of what are now known as BCS superconductors; although this theory did not explain the behavior of those superconductors, it is still fundamentally correct that a charged Bose condensate will be a superconductor. Such a state has never been observed experimentally. This would be a different mechanism from earlier proposals for exciton-mediated superconductivity; in one proposal [5], it was argued that the presence

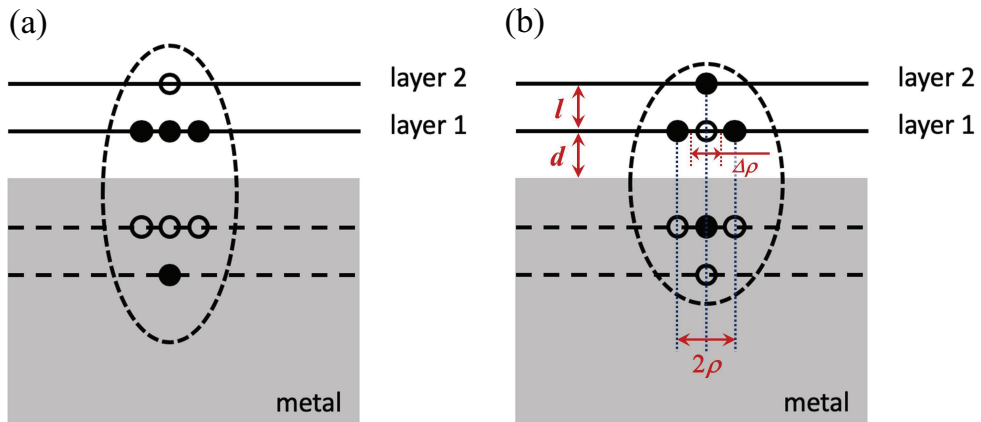


FIG. 1. a) Quaternion geometry proposed in Ref. [1]. The gray region indicates the metallic layer with image charge. b) Symmetric quaternion geometry considered here. See text for notations.

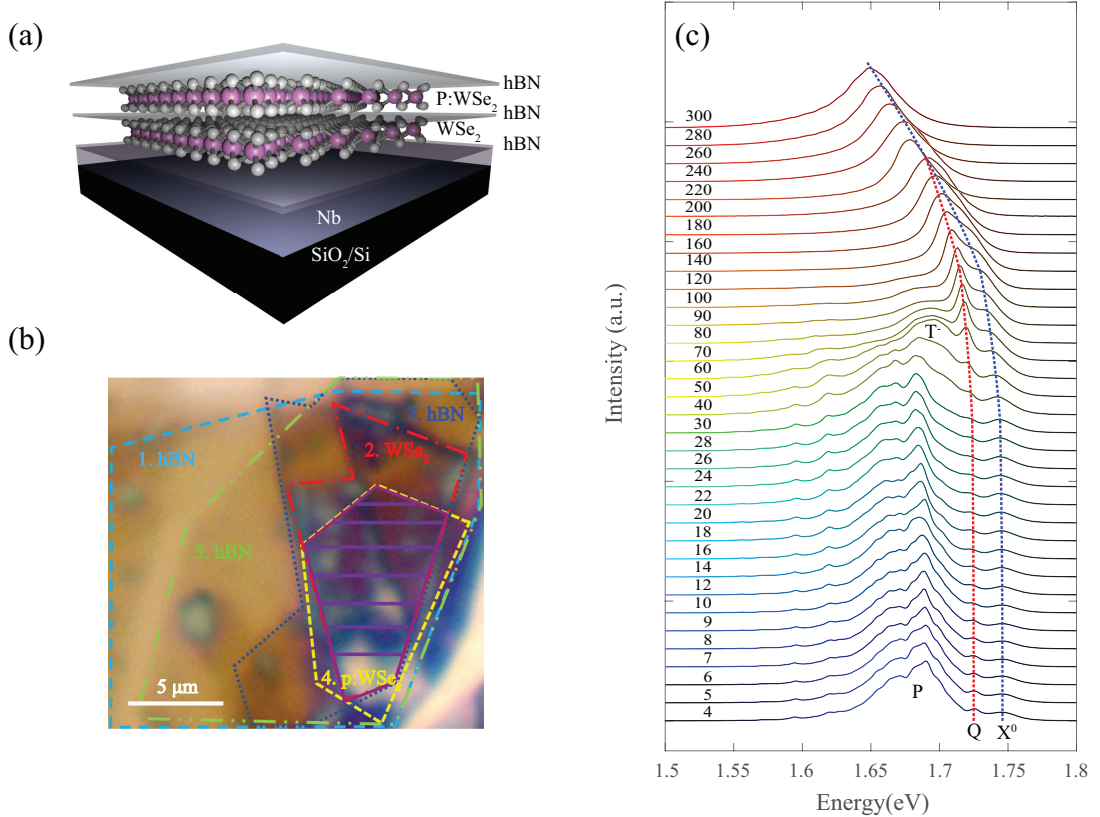


FIG. 2. a) Illustration of the fabricated structure. b) Image of the structure, with the layers labeled. c) Normalized photoluminescence spectrum at various temperatures. The dashed lines are fits to the Varshni equation for band gap shift of the lines, discussed in the Supplementary Information file.  $X^0$  = exciton,  $T^-$  = trion, P = impurity lines, and Q = the candidate for the quaternion emission. The doping density for the p:WSe<sub>2</sub> is  $\sim 10^{17-18} \text{ cm}^{-3}$  (Nb dopant).

of a magnetic field would cause neutral excitons to respond to an electric field; in another proposal [6], exciton-polaritons were proposed to play the same role as phonons in Cooper pairs.

Like a Bose condensate of excitons, a Bose condensate of quaternions would be metastable to recombination and require optical pumping for steady state. But as the burgeoning field experimental and theoretical work on Bose condensates of exciton-polaritons has shown [7–11], such a steady-state, optical pumped system can indeed undergo condensation, including the effects of superfluidity, and can reach equilibrium in steady state with a well-defined temperature [12, 13]. The quaternion particles discussed here do not have a polariton nature,

and therefore are more similar to pure exciton condensates, such as interlayer excitons in bilayer systems [14–16], which are subject to much greater disorder effects. However, since the quaternions have charge, they will have much stronger interactions, which may cause a condensate of such particles to be more readily in the Thomas-Fermi regime with a common chemical potential which smooths out disorder effects.

We consider a variant of the Yudson geometry, which is structurally a trion in one layer bound to a free carrier in a parallel layer, as shown in Figure 1(b). Our calculations, discussed below, indicate that this complex is more stable than the Yudson geometry. For the experiments, we fabricated the structure shown in Figure 2(a), based on two-dimensional monolayers of transition-metal dichalcogenides (TMDs). While the original proposal by Yudson was for III-V semiconductor quantum wells, TMD bilayer systems have a number of advantages. First, the intrinsic exciton binding energy is much larger, of the order of hundreds of meV, and therefore the excitons are stable at room temperature; in the WSe<sub>2</sub> layers used here, the exciton binding energy has been found experimentally to range from 0.1 to 0.8 eV [17–19], depending on the dielectric constant of the surrounding material. Also, hexagonal boron nitride (hBN) can be used as a good insulating barrier to prevent tunneling current while still allowing Coulomb interaction between free carriers in the layers [20].

We used niobium as the metal, with a spacer layer of 15 nm of hBN between the metal and the first TMD monolayer, a 7-nm spacer between the layers, and a capping hBN layer. Figure 2(b) shows an image of the stack of layers, and Figure 2(c) shows the photoluminescence (PL) spectrum as temperature is varied. As seen in the PL, a line appears, which we label Q, between the direct exciton line and the trion line, both of which have well-identified energies in these TMD monolayers. As shown below, the energy of the Q line is consistent with calculations of the quaternion binding energy.

We have reproduced this behavior in a second sample (Figure S1 of the Supplementary Information file), and we have examined a number of control structures, with the data given in the supplementary file for this publication. The control experiments can be summarized as follows:

- The monolayer exciton and trion lines are easily identifiable from comparison to samples with only monolayers. In a single, undoped monolayer of WSe<sub>2</sub> encapsulated in hBN, with no metal layer, we see the same direct exciton line, with energy about 15

meV higher than when there is a metal layer, with no quaternion line and very low trion emission (Figure S2 of the Supplementary Information file). In a single, *p*-doped monolayer of WSe<sub>2</sub> encapsulated in hBN, with no metal layer, the direct exciton line appears nearly at the same energy, with no quaternion line, and a relatively strong trion emission is seen (Figure S3 of the Supplementary Information file).

- In a single, *p*-doped monolayer of WSe<sub>2</sub> encapsulated in hBN in the presence of a metal layer, we see the direct exciton energy at nearly exactly the same energy as in the full bilayer stack with metal, and we see the strong trion line shifted lower by about 30 meV than in the full bilayer stack (Figure S4 of the Supplementary Information file), consistent with the theory presented here.
- In bilayer structures with and without a metal layer, the appearance of an indirect (interlayer) exciton line is a strong function of the thickness of the hBN layer between the TMD layers; for a 2-nm layer the indirect exciton line appears prominently (Figure S5 of the Supplementary Information file), while for a 7-nm layer, as used in the structure of Figure 2 presented here, there is no discernible indirect exciton line. The identification of the indirect exciton line in this and other samples was confirmed by lifetime measurements showing it has much longer lifetime than the direct exciton [21].
- The quaternion Q line appears *only* in the two samples with the full bilayer structure with the parallel metal layer (Figure 2(c) here, and Figure S1 of the Supplementary Information file). In a full bilayer structure without the metal layer, the quaternion line does not appear (Figure S5 of the Supplementary Information file).

The change of intensity of the Q line as temperature changes may be explained by several effects. First, for a quaternion to be formed, an exciton must find two free electrons (or holes), which means that their relative numbers will be determined by a mass-action equation [22]. Second, the number of free carriers will change as a function of temperature; at low temperature, these carriers will mostly be bound to impurities, and therefore the trion and quaternion intensities will drop. Third, at high temperature, all of the PL lines undergo thermal broadening, which makes it hard to distinguish one line from another.

These results, and the identification of the Q line as a quaternion, are consistent with the straightforward theory based on the configuration space method of the binding energy calcu-

lation for exciton complexes [23], which we present below with the additional inclusion of the added image charges in the metal layer. The configuration space method was recently proven to be efficient for the binding energy calculations as applied to quasi-1D [24] and quasi-2D bilayer semiconductors [25, 26] where it offers easily tractable analytical solutions [23]. The method itself was originally pioneered by Landau [27], Gor'kov and Pitaevski [28], and Holstein and Herring [29] in their studies of molecular binding and magnetism. The method provides an upper bound for the ground-state binding energy and captures essential kinematics of the formation of the complex, helping understand the general physical principles that underlie its stability.

We proceed from the assumption that, as shown in Fig. 1(b), the in-plane (intralayer, direct) trion makes the “core” to attach a like charge from the other monolayer to form the quaternion complex we observe. The reason for this assumption is that the axial symmetry of such a complex relative to the axis perpendicular to the bilayer, supplemented by the image charges of the same symmetry in the metallic layer, makes its ground-state coordinate wave function even (no nodes). From general quantum mechanics, in order for a quantum system to remain stable its ground-state wave function must have no nodes [27]. Hence, we start with the intralayer trion binding energy calculation in the presence of image charges. In the configuration space approach a singly charged exciton complex, the negative  $X^-$  or positive  $X^+$  trion, is regarded as a bound system of two equivalent excitons sharing the same hole (or electron) [23]. The trion bound state forms due to the exchange under-barrier tunneling between the equivalent configurations of the electron-hole system in the configuration space of the two independent relative electron-hole motion coordinates representing the two equivalent excitons separated by the center-of-mass-to-center-of-mass distance  $\Delta\rho$  as sketched in Fig. 1(b). The exchange tunneling rate integral  $J_{X^\pm}(\Delta\rho)$  controls the binding strength. The binding energy of the trion ground state is given by [25]

$$E_{X^\pm} = -J_{X^\pm}(\Delta\rho = \Delta\rho_{X^\pm}) \quad (1)$$

with  $\Delta\rho_{X^\pm}$  obtained variationally to maximize the tunneling rate. Originally developed for the exciton complexes formed by interlayer (indirect) excitons [25, 26], this approach remains valid in the case of the zero interlayer distance as well, to give the tunneling rate integral for

the direct intralayer trion as follows [26]

$$J_{X^\pm}(\Delta\rho) = 2^{10} e^{-4\Delta\rho} \Delta\rho \left[ 1 + \frac{\Delta\rho}{4 \left( r_0 + \left\{ \frac{1}{\sigma} \right\} \Delta\rho / \lambda \right) (2\Delta\rho - 1)} \right] \frac{\lambda \Delta\rho}{\left( \frac{r_0 + \left\{ \frac{1}{\sigma} \right\} \Delta\rho / \lambda}{r_0 + \Delta\rho} \right) \left\{ \frac{\sigma}{1} \right\} (2\Delta\rho - 1)} \quad (2)$$

Here, the upper or lower term should be taken in the curly brackets for the positive or negative trion, respectively. The 3D “atomic units” are used [27–29] with distance and energy measured in units of the exciton Bohr radius  $a_B^* = 0.529 \text{ \AA} \varepsilon / \mu$  and exciton Rydberg energy  $Ry^* = \hbar^2 / (2\mu m_0 a_B^{*2}) = 13.6 \text{ eV} \mu / \varepsilon^2$ , respectively, where  $\varepsilon$  represents the effective average dielectric constant of the heterostructure and  $\mu = m_e / (\lambda m_0)$  stands for the exciton reduced effective mass (in units of the free electron mass  $m_0$ ) with  $\lambda = 1 + \sigma$  and  $\sigma = m_e / m_h$ . To properly take into account the screening effect for the three charges confined in the monolayer, we use the Keldysh-Rytova interaction potential (see Ref. [30]) with  $r_0 = 2\pi\chi_{2D}$  representing the screening length parameter where  $\chi_{2D}$  is the in-plane polarizability of the 2D material [31, 32]. Seeking the extremum for  $J_{X^\pm}(\Delta\rho)$  in the physically significant region  $\Delta\rho > 1$  can be done with *only* the leading terms in small  $1/\Delta\rho$  included in the procedure. This gives [26]

$$\Delta\rho_{X^\pm} = \frac{13 - \left\{ \frac{\sigma}{1/\sigma} \right\}}{8} - \left( 3 + 2 \left\{ \frac{\sigma}{1/\sigma} \right\} \right) r_0. \quad (3)$$

Substituting this in Eq. (2), one obtains the binding energies per Eq. (1) for the positive and negative direct trion in a single monolayer in the absence of a metal.

In the presence of a metal, the total potential energy of the intralayer trion is

$$U(\rho, d) = U_0(\rho) + 2 \left( \frac{4}{\sqrt{(2d)^2 + \rho^2}} - \frac{2}{\sqrt{(2d)^2 + (2\rho)^2}} - \frac{3}{2d} \right), \quad (4)$$

where  $\rho$  is the distance between the hole and the electron in the monolayer shown in Fig. 1(b) and  $U_0(\rho)$  is the electron-hole potential interaction energy in the absence of a metal which is already included in Eq. (2). The extra second term comes from the image charge interaction with  $d$  being the distance of the monolayer from the metal (the distance between the image and the original). This term is seen to increase the trion binding energy. For the quaternion,

in a similar manner, the total potential energy with the image charge interaction included is

$$U(\rho, d, l) = U_0(\rho) + 2 \left( \frac{4}{\sqrt{(2d)^2 + \rho^2}} - \frac{2}{\sqrt{(2d)^2 + (2\rho)^2}} - \frac{3}{2d} \right. \\ \left. + \frac{2}{\sqrt{l^2 + \rho^2}} - \frac{1}{l} + \frac{2}{2d + l} - \frac{1}{2d + 2l} - \frac{4}{\sqrt{(2d + l)^2 + \rho^2}} \right), \quad (5)$$

where in addition to  $d$  and  $\rho$  defined above,  $l$  is the thickness of the spacer layer between the two TMD monolayers — see Fig. 1(b).

Next, we look at the recombination energies to be able to interpret the PL emission spectra in Fig. 2(c) in terms of Eqs. (1)–(5). Our main task is to explain the position of the Q line, which shows up and stays firmly there in the presence of a metal, relative to the direct exciton emission line ( $X^0$ ) and the intralayer trion line ( $T^-$ ). Our room-temperature exciton emission line  $X^0$  is positioned at 1.65 eV, which exactly corresponds to the room-temperature WSe<sub>2</sub> bandgap of 1.89 eV and the exciton binding energy of 240 meV reported recently from precision measurements [19]. We also observe the  $T^-$  line shifted lower by 30 meV relative to the  $X^0$  line. We note that the  $X^0$  line can only be affected negligibly by the presence of a metal due to the overall exciton neutrality, as opposed to the  $T^-$  and Q lines, which makes the set of Eqs. (1)–(5) sufficient to complete our task. The PL photon energy is given by the initial energy minus the final energy. In the exciton recombination process, the final state is nothing, so the energy of the photon emitted is the bandgap minus the exciton binding energy in the presence of a metal. As discussed above, experimentally there is a very little (negligible)  $X^0$  line energy shift with or without the metal layer, which is a consequence of the exciton neutrality. For the intralayer trion, the final state is a single electron (or hole), which in the presence of a metal has the energy  $2[-1/(2d)]$  due to the image-charge interaction. For the quaternion, there are two final electrons (or two holes), and so for the same reason the final energy is  $2[-1/(2d) - 1/(2d + 2l)]$ . Subtracting these final state energies, together with  $U_0(\rho)$ , from  $U(\rho, d)$  and  $U(\rho, d, l)$  in Eqs. (4) and (5), respectively, and adding the intralayer trion binding energy with no metal present as given by Eqs. (1)–(3), we obtain the recombination energies of interest in the presence of a metal as functions of  $d$  and  $l$ , which in our experiment are equal to 15 nm and 7 nm, respectively.

Figure 3(a) shows the recombination energies for the intralayer trion and quaternion as functions of  $d$  and  $l$  calculated in atomic units (a.u.) with the screening parameter  $r_0 = 0.05$ .

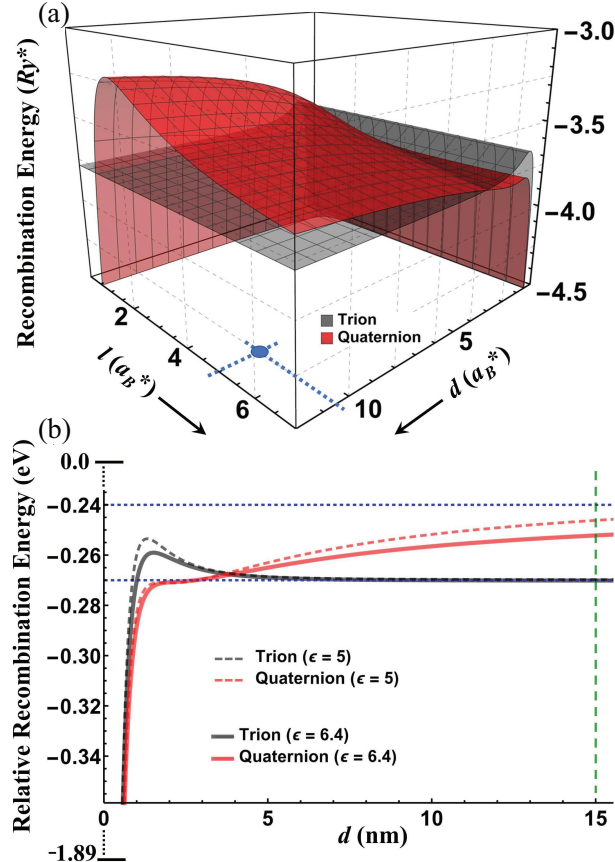


FIG. 3. (a) The recombination energies for the intralayer trion and quaternion as functions of  $d$  and  $l$  calculated in atomic units from Eqs. (1)–(5) with  $\sigma=1$  and  $r_0=0.05$ . The blue spot indicates our experimental  $d$  and  $l$  in these units (with  $\epsilon=6.4$ ). (b) The trion and quaternion recombination energies relative to the bandgap, calculated as functions of  $d$  in nanometers for the experimental value of  $l=7$  nm, with  $\epsilon=5$  (dashed lines) and  $\epsilon=6.4$  (solid lines), and  $m_e=m_h=0.48 m_0$ . The horizontal dotted blue lines trace the exciton binding energy of 240 meV [19] and the trion binding energy of 30 meV we observe. The vertical dashed green line traces  $d=15$  nm in our experiment. See text for details on the calculations and other material parameters used.

One can see that, apart from the domain of very short  $d$  and  $l$ , the quaternion recombination energy is always above that of the trion. Obviously, this comes from the fact that adding of an extra like-charge carrier to a charged three-particle system (intralayer trion) results in an extra repulsion in the entire four-particle complex. This lowers its binding energy to give an increase in the recombination energy. One can also see that the quaternion recombination energy goes slowly up as  $d$  increases, to exceed the exciton recombination energy for  $d$  large

enough ( $d = \infty$  corresponds to the no-metal situation), which would make it unstable to conversion down to excitons and/or trions. Thus, the intervening hBN layer thickness plays a crucial role, and we see all three recombination lines individually because our experimental conditions are different from those of Ref. [19], for example, where a TMD monolayer was placed directly onto a metal. The decrease of the screening parameter  $r_0$  shifts both surfaces in Fig. 3(a) up (not shown here) due to the trion (the “core” for both quaternion and trion) binding energy decrease caused by the increased repulsion of like charges in it.

Figure 3(b) shows the relative recombination energies for the trion and quaternion in eV, calculated as functions of the distance  $d$  from the nearest monolayer to the metal surface expressed in nanometers. This figure is the cross-section of Fig. 3(a) converted to physical units with  $l = 7$  nm and then shifted vertically by choosing the appropriate  $r_0$  value to match the 1.89 eV bandgap with the binding energies of 240 meV and 30 meV for the direct exciton and the intralayer trion, respectively. The figure is obtained for two values of the average effective dielectric constant of our system,  $\varepsilon = 5$  and  $\varepsilon = 6.4$ , to compare. The former would be taken if the dielectric response is dominated by the hBN value  $\varepsilon_{hBN} \simeq 5$  [33], while the latter appears to be more realistic in our case to also include a large dielectric permittivity  $\sim 13 - 14$  of the TMD layers themselves [31]. The effective masses are taken to be  $0.48 m_0$  for both electron and hole [34], to give  $\sigma = 1$  with equal binding energies for the positive and negative trions per Eqs. (1)–(3). With these material parameters we obtain  $a_B^* = 1.10$  nm,  $Ry^* = 0.13$  eV for  $\varepsilon = 5$ , and for the higher value of  $\varepsilon = 6.4$ , we obtain  $a_B^* = 1.41$  nm and  $Ry^* = 0.08$  eV. These values imply that the distance of  $l = 7$  nm corresponds to 6.35 in atomic units for  $\varepsilon = 5$ , and 4.96 in atomic units for  $\varepsilon = 6.4$ . These  $l$  values can then be used in Eq. (5) to eliminate the  $l$  variable from it, whereby Eqs. (1)–(5) provide the crosscuts of Fig. 3(a) as functions of  $d$  (with fixed  $r_0$ ) per the procedure described at the end of the previous paragraph. By using known values of  $a_B^*$  and  $Ry^*$ , these functions can be converted to physical units, followed by choosing the parameter  $r_0$  to vertically shift the curves obtained to match the WSe<sub>2</sub> bandgap energy structure. We find  $r_0 = 0.0124$  and  $0.043$ , in atomic units, for  $\varepsilon = 5$  and  $6.4$ , respectively. The relatively low  $r_0$  values we thus obtain are consistent with the experimental reports of the exciton emission linewidth approaching the homogeneous limit for TMD monolayers embedded in between thick hBN layers [35]. As seen in Fig. 3(b), both choices of  $\varepsilon$  put the quaternion line in between the trion and the exciton.

However, in the case of  $\varepsilon = 5$ , for the value of  $d = 15$  nm in our sample, the quaternion is too close to the exciton and so should hardly be resolvable experimentally. For  $\varepsilon = 6.4$ , all three lines are well separated in energy, in agreement with what we see in the PL spectra shown in Fig. 2(c). One can also see that increasing  $d$  pushes up the quaternion recombination energy to exceed that of the exciton, making the quaternion unstable as mentioned above.

All of the other lines which we do (or do not) observe spectroscopically can be identified as known lines, as follows:

- Impurity lines are seen even without the metal layer (Figures S2, S3, and S5 in the Supplementary Information file) at energies in agreement with previous work on 2D monolayers [36], and occur only at low temperature.
- The intralayer trion line showing up at 1.7 eV at elevated temperatures is well identified in other works [37] and occurs separately from the new line, and coexists with it (e.g., at  $T \sim 80 - 100$  K in Figure 2(c)).
- The intralayer biexciton line is well established [38] appear at lower energy than the intralayer trion line and should barely be affected by the presence of a metal due to the overall biexciton electroneutrality. We see evidence of this line in Figures S4 and S5 of the Supplementary Information file, where it is well separated from the Q line, and occurs at the same location with and without the metal layer.
- Interlayer exciton lines occur at much lower energy due to the band offset between the layers, because the PL photon emitted comes from an interlayer recombination process, as confirmed by other works [39] and our own work with related samples (Figure S5 of the Supplementary Information file, and Ref. [21]).
- Charged interlayer excitons, which we do not see, consisting of two holes in one monolayer, and one electron in the other layer (or vice versa), require a thinner interlayer spacer to be visible spectroscopically ( $\sim 1$  nm as opposed to 7 nm we have in the sample used for Figure 2) and will also have PL energy shifted down, below the interlayer exciton line, since they also require an interlayer photon recombination. They also have small binding energies ( $\sim 10 - 15$  meV demonstrated both theoretically and experimentally [25, 39]).

- Interlayer biexcitons require high excitation power and so far were not observed in TMD bilayers to our knowledge due to their vanishingly small binding energy [25]. They would not be stabilized by the presence of a metal either because of their overall electrical neutrality.
- The trion state formed by the exciton in one monolayer and a hole (or electron) in the other monolayer cannot show up in our spectra, as such a state possesses no intrinsic axial symmetry necessary for it to be stable. From general quantum mechanics, the ground state of a stable quantum system must have no nodes [27]. For a few-particle complex to be stable, the coordinate wave function of the complex has to be even (no nodes), which in our case can only occur if the complex has an axially symmetric charge distribution relative to the axis perpendicular to the bilayer. This is one of the main features of the quaternion complex we claim to observe, and what is totally absent from such a trion complex. Adding a metal does not change the symmetry and so does not help stabilize this state.

In conclusion, the existence of doubly-charged excitonic complexes, or quaternions, in bilayer TMD structures near metallic layers, is to be expected from theoretical calculations, which show that this complex is quite robust to variation of the material parameters and layer distances. Our spectroscopic studies, summarized in Fig. 2 for WSe<sub>2</sub> bilayer structures near niobium metal and in the Supplementary Information file for the control samples, give a candidate spectral line in full agreement with the theory predictions. Further confirmation of the existence of this state may be obtained by observing motion of them in response to an in-plane electric field, since they have net charge, or by two-dimensional spectroscopy methods.

The question remains what would be needed to have a realistic room temperature superconductor made from a condensate of these complexes. Bose condensation occurs generally at high density, which means that experiments with high excitation intensity could push the density high enough for condensation, but collisional Auger nonradiative recombination may deter this. In general, it has been difficult to see coherent light emission, i.e., spectral narrowing and increase of the temporal coherence as seen in interferometry, from indirect exciton condensates, which is the primary telltale for exciton condensation. It may be that

mixing these quaternion states resonantly with photons to create a polaritonic state may be the best path toward condensation; the polariton effect also reduces the effective mass of the particles, which reduces the needed density for condensation and also averages over disorder on length scales of the wavelength of light. Our results here indicate, in any case, that quaternion physics in bilayer systems with metal layers is a promising field of research.

**Acknowledgements.** This work was supported by the US Army Research Office under MURI award W911NF-17-1-0312 (Z.S., J.B, D.W.S.) and by the U.S. Department of Energy, Office of Science, Office of Basic Energy Sciences, under award number DE-SC0007117 (I.V.B). K.W. and T.T. acknowledge support from the EMEXT Element Strategy Initiative to Form Core Research Center, Grant Number JPMXP0112101001 and the CREST(JPMJCR15F3), JST. B.M.H. and Q.C. were supported by the Department of Energy under the Early Career Award program (#DE-SC0018115).

---

[1] V.I. Yudson, Phys. Rev. Lett. **77**, 1564 (1996).

[2] F. Pulizzi, D. Sanvitto, P.C.M. Christianen, A.J. Shields, S.N. Holmes, M.Y. Simmons, D.A. Ritchie, M. Pepper, and J.C. Maan, Phys. Rev. B **68**, 205304 (2003).

[3] Z. Li, T. Wang, Z. Lu, C. Jin, Y. Chen, Y. Meng, Z. Lian, T. Taniguchi, K. Watanabe, S. Zhang, D. Smirnov and S.-F. Shi, Nature Comm. **9**, 3719 (2018).

[4] M.R. Schafroth, Physical Review **96**, 1442 (1954).

[5] Yu.E. Lozovik and V. Yudson, Sov. Phys. JETP. **44**, 389 (1976).

[6] O. Cotlet, S. Zeytinoglu, M. Sigrist, E. Demler, and A. Imamoglu, Phys. Rev. B **93**, 054510 (2016).

[7] J. Kasprzak, M. Richard, S. Kundermann, A. Baas, P. Jeanbrun, J.M.J. Keeling, R. André, J.L. Staehli, J.L., V. Savona, P.B. Littlewood, B. Deveaud, and L.S. Dang, Nature **443**, 409 (2006).

[8] R. Balili, V. Hartwell, D.W. Snoke, L. Pfeiffer and K. West, Science **316**, 1007 (2007).

[9] H. Deng, H. Haug, and Y. Yamamoto, Rev. Mod. Phys. **82**, 1489 (2010).

[10] I. Carusotto and C. Ciuti, Rev. Mod. Phys. **85**, 299 (2013).

[11] D. Snoke and J. Keeling, Physics Today **70**, 54 (2017).

[12] Y. Sun, P. Wen, Y. Yoon, G.-Q. Liu, M. Steger, L.N. Pfeiffer, K. West, D.W. Snoke, and K.A. Nelson, Phys. Rev. Lett. **118**, 016602 (2017).

[13] D. Caputo, D. Ballarini, G. Dagvadorj, C. Sánchez Muñoz, M. De Giorgi, L. Dominici, K. West, L.N. Pfeiffer, G. Gigli, F.P. Laussy, M.H. Szymanska, and D. Sanvitto, Nature Materials **17**, 145 (2018).

[14] M. Combescot, R. Combescot, and F. Dubin, Rep. Prog. Phys. **80**, 066501 (2017).

[15] Yu.E. Lozovik, Physics Uspekhi **61**, 1094 (2018).

[16] D.W. Snoke, in *Quantum Gases: Finite Temperature and Non-Equilibrium Dynamics*, N.P. Proukakis, S.A. Gardiner, M.J. Davis, and M.H. Szymanska, eds. (Imperial College Press, London, 2013).

[17] K. He, N.Kumar, L. Zhao, Z. Wang, K.F. Mak, H. Zhao, and J. Shan Phys. Rev. Lett. **113**, 026803 (2014).

- [18] A.T. Hanbicki, M. Currie, G. Kioseoglou, A.L. Friedman, and B.T. Jonker, Solid State Comm. **203**, 16 (2015).
- [19] S. Park, N. Mutz, T. Schultz, S. Blumstengel, A. Han, A. Aljarb, L.-J. Li, E.J.W. List-Kratochvil, P. Amsalem, and N. Koch, 2D Mater. **5**, 025003 (2018).
- [20] A. Raja, A. Chaves, J. Yu, G. Arefe, H.M. Hill, A.F. Rigos, T.C. Berkelbach, P. Nagler, C. Schller, T. Korn, C. Nuckolls, J. Hone, L.E. Brus, T.F. Heinz, D.R. Reichman, and A. Chernikov, Nature Comm. **8**, 8, 15251 (2017).
- [21] Z. Sun, J. Beaumariage, Q. Cao, K. Watanabe, T. Taniguchi, B. Hunt, and D.W. Sroka, (arXiv:2001.01009).
- [22] D.W. Sroka, *Solid State Comm.* **146**, 73 (2008).
- [23] I.V. Bondarev, Mod. Phys. Lett. B **30**, 1630006 (2016).
- [24] I.V. Bondarev, Phys. Rev. B **83**, 153409 (2011); Phys. Rev. B **90**, 245430 (2014).
- [25] I.V. Bondarev and M.R. Vladimirova, Phys. Rev. B **97**, 165419 (2018).
- [26] I.V. Bondarev, O.L. Berman, R.Ya. Kezerashvili, and Y.E. Lozovik, arXiv:2002.09988.
- [27] L.D. Landau and E.M. Lifshitz, *Quantum Mechanics. Non-Relativistic Theory* (Pergamon, Oxford, 1991).
- [28] L.P. Gor'kov and L.P. Pitaevski, Dokl. Akad. Nauk SSSR **151**, 822 (1963) [English transl.: *Soviet Phys.—Dokl.* **8**, 788 (1964)].
- [29] C. Herring, Rev. Mod. Phys. **34**, 631 (1962); C. Herring and M. Flicker, Phys. Rev. **134**, A362 (1964).
- [30] L.V. Keldysh, Sov. Phys. JETP **29**, 658 (1979); N.S. Rytova, Proc. MSU Phys. Astron. **3**, 30 (1967).
- [31] T.C. Berkelbach, M.S. Hybertsen, and D.R. Reichman, Phys. Rev. B **88**, 045318 (2013).
- [32] P. Cudazzo, I.V. Tokatly, and A. Rubio, Phys. Rev. B **84**, 085406 (2011).
- [33] A. Laturia, M.L. Van de Put, and W.G. Vandenberghe, 2D Materials and Applications **2**, 6 (2018).
- [34] F.A. Rasmussen and K.S. Thygesen, J. Phys. Chem. C **119**, 13169 (2015).
- [35] F. Cadiz, E. Courtade, C. Robert, G. Wang, Y. Shen, H. Cai, T. Taniguchi, K. Watanabe, H. Carrere, D. Lagarde, M. Manca, T. Amand, P. Renucci, S. Tongay, X. Marie, and B. Urbaszek, Phys. Rev. X **7**, 021026 (2017).

- [36] Z. Wang, Y.-H. Chiu, K. Honz, K.F. Mak, and J. Shan, *Nano. Lett.* **18**, 137 (2018).
- [37] A. Arora, M. Koperski, K. Nogajewski, J. Marcus, C. Faugerasa. and M. Potemski, *Nanoscale* **7**, 10421 (2015).
- [38] Y. You, X.-X. Zhang, T.C. Berkelbach, M.S. Hybertsen, D.R. Reichman, and T.F. Heinz, *Nature Physics* **11**, 477 (2015).
- [39] L.A. Jauregui, A.Y. Joe, K. Pistunova, D.S. Wild, A.A. High, Y. Zhou, G. Scuri, K. De Greve, A. Sushko, C.-H. Yu, T. Taniguchi, K. Watanabe, D.J. Needleman, M.D. Lukin, H. Park, and P. Kim, *Science* **366**, 870 (2019).